Check for updates

Received: 9 November 2023 | Revised: 27 June 2024 | Accepted: 1 July 2024

DOI: 10.1111/jns.12645

RESEARCH REPORT

WILEY

# Initial findings using high-resolution magnetic resonance imaging for visualisation of the sural nerve and surrounding anatomy in healthy volunteers at 7 Tesla

Amy R. McDowell[1] | Laura Zambreanu[1,2] | Hamza A. Salhab[1] | Carolynne M. Doherty[1] | Philippa Bridgen[3,4,5] | Pete Lally[6] | Sachit Shah[1,2] | Zimu Huo[6] | Stephen J. Wastling[2] | Tarek Yousry[1,2] | Jasper Morrow[1,2] | John S. Thornton[1,2] | Michael P. Lunn[1,2,7]

[1]UCL Queen Square Institute of Neurology, London, UK

[2]Centre for Neuromuscular Diseases, National Hospital for Neurology and Neurosurgery, London, UK

[3]Biomedical Engineering Department, School of Biomedical Engineering and Imaging Sciences, King's College London, London, UK

[4]London Collaborative Ultra High Field System (LoCUS), Kings College London, London, UK

[5]Guys and St Thomas' NHS Foundation Trust, Kings College London, London, UK

[6]Imperial College London, London, UK

[7]NIHR University College London Hospitals Biomedical Research Centre, Research & Development, London, UK

**Correspondence**
Amy R. McDowell, Department of Neuromuscular Disease, Institute of Neurology, Queen Square, London, UK.
Email: a.mcdowell@ucl.ac.uk

**Funding information**
Muscular Dystrophy UK; NIHR Biomedical Research Centre at University College London Hospitals NHS Foundation Trust and University College London

[Correction added on 01 August 2024, after first online publication: The surname of the fourth author has been corrected in this version.]

## Abstract

**Background and Aims:** Histopathological diagnosis is the gold standard in many acquired inflammatory, infiltrative and amyloid based peripheral nerve diseases and a sensory nerve biopsy of sural or superficial peroneal nerve is favoured where a biopsy is deemed necessary. The ability to determine nerve pathology by high-resolution imaging techniques resolving anatomy and imaging characteristics might improve diagnosis and obviate the need for biopsy in some. The sural nerve is anatomically variable and occasionally adjacent vessels can be sent for analysis in error. Knowing the exact position and relationships of the nerve prior to surgery could be clinically useful and thus reliably resolving nerve position has some utility.

**Methods:** 7T images of eight healthy volunteers' (HV) right ankle were acquired in a pilot study using a double-echo in steady-state sequence for high-resolution anatomy images. Magnetic Transfer Ratio images were acquired of the same area. Systematic scoring of the sural, tibial and deep peroneal nerve around the surgical landmark 7 cm from the lateral malleolus was performed (number of fascicles, area in voxels and $mm^2$, diameter and location relative to nearby vessels and muscles).

**Results:** The sural and tibial nerves were visualised in the high-resolution double-echo in steady-state (DESS) image in all HV. The deep peroneal nerve was not always visualised at level of interest. The MTR values were tightly grouped except in the sural nerve where the nerve was not visualised in two HV. The sural nerve location

This is an open access article under the terms of the Creative Commons Attribution License, which permits use, distribution and reproduction in any medium, provided the original work is properly cited.
© 2024 The Author(s). *Journal of the Peripheral Nervous System* published by Wiley Periodicals LLC on behalf of Peripheral Nerve Society.

was found to be variable (e.g., lateral or medial to, or crossing behind, or found positioned directly posterior to the saphenous vein).

**Interpretation:** High-resolution high-field images have excellent visualisation of the sural nerve and would give surgeons prior knowledge of the position before surgery. Basic imaging characteristics of the sural nerve can be acquired, but more detailed imaging characteristics are not easily evaluable in the very small sural and further developments and specific studies are required for any diagnostic utility at 7T.

**KEYWORDS**

7T MRI, fascicles, neurography, peripheral nerve imaging, sural nerve biopsy

## 1 | INTRODUCTION

Visualisation of peripheral nerves in vivo with magnetic resonance imaging (MRI) and ultrasound (US) has become increasingly possible as resolution of these techniques has improved.[1] The pathological imaging characteristics of peripheral nerves have been described in many diseases, acquired and genetic, by US and MRI, with the latter being limited to more proximal, larger nerves and tumours and masses. At present, the clinical diagnostic utility of MRI and US is limited in inflammatory and infiltrative diseases because of the lack of specificity of the findings, reducing the discriminating ability of those techniques.

In focal compressive lesions of distal peripheral nerves, such as carpal tunnel syndrome, the benefits of US diagnosis are real and obvious and can guide intervention or alternative strategies. US is also currently far superior for more distal and superficial imaging, with better resolution when nerves are more superficial than deep (0.08–0.3 mm for US vs. 1-2 mm in MRI),[2] but it still has limitations of spatial resolution and differentiating the diagnostic characteristics in some pathological conditions. In focal lesions of more proximal neural structures, such as thoracic outlet syndrome,[3] nerve sheath tumours or intra-neural perineuromas,[4] MRI can be diagnostic, but both US and MRI are used in a Bayesian decision process after clinical assessment. In inflammatory (e.g., chronic inflammatory demyelinating polyradiculoneuropathy [CIDP] and Guillain-Barré syndrome [GBS], infiltrative (lymphoma or amyloid) and some hereditary neuropathies, imaging can again be performed as part of a diagnostic work-up. However the imaging features, such as heterogeneous nerve swelling, generalised thickening or intraneural signal abnormalities do not definitively differentiate between those diseases which are part of their differential diagnosis.[5] For example, the imaging features of nerve thickening and enhancement which appear within diagnostic criteria for CIDP also occur in hereditary demyelinating neuropathies, Polyneuropathy, Organomegaly, Endocrinopathy, Myeloma protein, and Skin changes (POEMS) syndrome, multifocal motor neuropathy, neurolymphomatosis and others. Finding diagnostic intraneural pathological correlates which are specific for particular diseases using non-invasive imaging is one of our aims that might obviate the need for a sural nerve biopsy in some cases if distinction could be made non-invasively.

Histopathological diagnosis is the gold standard in many inflammatory and infiltrative peripheral nerve diseases, and a sensory nerve biopsy of sural or superficial peroneal nerve is favoured for both site and size when and if a nerve biopsy is required. Positive diagnoses can be made or confirmed in CIDP, amyloid, vasculitis, sarcoid, neurolymphomatosis, some inherited neuropathies (whole genome screening has superseded this) and others. A nerve biopsy is not always possible nor definitively diagnostic. Furthermore, conditions with no sensory nerve involvement such as multifocal motor neuropathy with conduction block or motor neurone disease present no biopsy opportunity. Neither sural nor superficial peroneal nerve biopsy is technically difficult, but the anatomical siting of the sural nerve, close and variably related to neighbouring vessels, sometimes results in an artery being sent for histopathology. Therefore, knowing the exact position and relationships of the nerve prior to surgery and being able to detect a macroscopic segment of nerve to biopsy perhaps a few centimetres proximal or distal to a normal target site could potentially be clinically useful. Knowing the intra-neural imaging characteristics of demyelination in a sensory nerve might well be applicable to less accessible sensory nerves or motor nerves where no sensory involvement is present. In future, we would hope that with validation of MRI indices and histological comparison to pathological specimens, it may be possible to extrapolate those findings to the ('unbiopsiable') tibial nerve or sciatic nerve to establish independently diagnostic criteria. Those might be detected at lower field strengths and reduce or remove the need for biopsy altogether.

At field strengths of 3T, MRI imaging of peripheral nerves is often limited to large proximal nerves of several millimetres in diameter with multiple fascicles. At the very best levels of 3T resolution, the fascicles in these large nerves can just about be counted, and basic information about signal and enhancement characteristics in cross- and longitudinal-section is available. The sural nerve has previously been investigated at 3T.[6] Kollmer et al. used magnetic resonance neurography (MRN) to detect and quantify lesions of the sural nerve in symptomatic and asymptomatic transthyretin familial amyloid polyneuropathy and controls in correlation with electrophysiologic and histopathologic findings. Images were acquired at the mid-thigh to ankle level; however, in controls, sural nerve segmentation was not possible beyond the proximal third of the lower leg. Their results were

15298027, 2024, 3, Downloaded from https://onlinelibrary.wiley.com/doi/10.1111/jns.12645 by Test, Wiley Online Library on [13/09/2024]. See the Terms and Conditions (https://onlinelibrary.wiley.com/terms-and-conditions) on Wiley Online Library for rules of use; OA articles are governed by the applicable Creative Commons License

sensitive to the differences between controls and patients ($p < .0001$) and controls and carriers ($p = .0065$) in the *proximal* sural nerve.

We have successfully investigated the feasibility of high-resolution anatomical and quantitative MRI assessment of sciatic nerve fascicles in patients with Charcot-Marie-Tooth (CMT) 1A at 7T previously.[7] The 7T imaging presents the opportunity to image the distal sural nerve at ankle level (a diameter between 2.7 and 3.4 mm; mean = 3.22 mm[8]). Prior publication of distal 7T neurography is limited to a study on one healthy volunteer (HV)[9] and a case report,[10] both of which imaged the larger tibial nerve. There are no studies to our knowledge of the sural nerve at the ankle. We present here our feasibility study in visualising the sural nerve.

## 2 | MATERIALS AND METHODS

Eight healthy control volunteers (three male, five female, average age 37 years [range, 27–54]) without any history of muscle disease or MR contraindications were enrolled after an informed consent procedure. Magnetic resonance images were acquired on high-field 7T Terra MRI Scanner (Siemens Healthcare, Erlangen, Germany) using a 28-channel transmit-receive QED knee coil.

Scans included a double-echo in steady-state (DESS) sequence, which is a three-dimensional (3D) gradient-spoiled MRI sequence with good musculoskeletal tissue contrast.[11] In our previous work,[7] DESS images showed high signal-to-noise ratio (SNR), high resolution and most importantly good fat suppression to delineate the sural nerve from the surrounding fat. Fat suppression provided by this sequence enhanced visualisation of the sural nerve as it is located in the superficial fat of the lower leg. At 3T non-fat suppressed sequences are recommended[1] as the absence of the signal in the nerve is contrasted against the high signal in the fat, helping to identify the likely location of the sural nerve. However, due to the higher SNR at 7T, we can examine the signal from the sural nerve itself rather than its absence, and we therefore sought to remove any other less relevant signals.

We performed axial scans with an in-plane resolution of $0.1483 \times 0.1483\ mm^2$ and a field of view (FoV) of $140 \times 140\ mm^2$; TR = 24.79 ms; echo time (TE) = 7.55 ms; flip angle = 13°; $80 \times 2$ mm thick slices; distance factor 20%; readout bandwidth = 204 Hz/pixel; anterior/posterior phase encoding direction and 2× parallel imaging resulting in a scan time of 12:38 min.

Quantitative magnetisation transfer ratio [MTR] imaging was also performed for the first time in the sural nerve. Axial scans in the same plane as the DESS sequences were performed with a voxel size of $0.5 \times 0.5\ mm^2$; FoV $160 \times 160\ mm^2$; TR = 62.0 ms; TE = 6.32 ms; flip angle = 25°; $80 \times 2$ mm slices; distance factor 20%; readout bandwidth = 190 Hz/pixel; anterior/posterior phase encoding direction and 3× parallel imaging resulting in a scan time of 8:15 min with magnetisation transfer preparation pulse and a second scan with the same parameters without a magnetisation preparation pulse. The MTR was calculated using the equation $MTR = MT_{off}–MT_{on}/MT_{off}$.

Participants were positioned feet first supine, with the malleoli at the bottom of the coil, with the foot positioned in a plantar flexion position. Sandbags and a Pearltec multipad (https://www.pearl-technology.ch/en/multipad) prevented foot and lower leg movement. Three localisers were acquired, and a 3D T1-weighted image was used to identify the sural nerve.

A multi-planar reconstruction (MPR) was created from the T1 to orientate the axial slices perpendicular to the sural nerve, and this image position was then copied for all following sequences. The research MR radiographer (9 years experience) identified the orientation of the sural nerve to ensure clear axial images and copied this positioning to all further scans.

Segmentations were performed independently by one of the authors (H.S.), under the supervision of a neuroradiologist and a neurologist with extensive neuromuscular imaging experience (S.S. and J.M.). The ankle joint (lateral malleolus) was identified in the high-resolution anatomy scan, and all measurements were calculated from this point. Every fifth slice was segmented starting 25 slices superior to the lateral malleolus (when the nerves became visible); eight slices were analysed in total with three regions of interest (ROIs) for the tibial nerve, deep peroneal nerve and sural nerve respectively. ROIs were drawn on the axial DESS scans in ITKsnap (http://www.itksnap.org) using the paintbrush tool. Nerve and fascicle regions were subjectively defined with the nerve borders based on visual appreciation of significant contrast between the area and surrounding tissue taking into consideration the nerve/fascicles course on the other slices. Nerve diameters were recorded as the maximal axial diameter that could be measured on each slice, and the cross-sectional area was measured for the tibial nerve using the enclosing ROI segmentation. Fascicles were counted when they were confidently identified.

## 3 | RESULTS

Axial images 7.2 cm above the lateral malleolus from all eight participants are shown in Figure 1. Images were chosen to demonstrate the location and relationship of the small saphenous vein and sural nerve at this level which is the usual site for biopsy. In all volunteers, the sural nerve was easily visualised and distinguishable from the vein. The orientation of the nerve and vein to each other is variable, although they are generally closely located.

Example coronal images are shown in Figure 2. These demonstrate the excellent visualisation of the course of the sural nerve relative to the saphenous vein. Images are again centred at 7.2 cm above the lateral malleolus.

Table 1 is a summary of the systematic scoring concentrating on the area around the landmark 7.2 cm from the lateral malleolus. The full table can be found in Table S1. Although the sural nerve was readily visualised, there was not enough resolution to accurately estimate the number of fascicles contained therein.

Figure 3 shows graphs of MTR in the three nerves seen at 7.2 cm above the malleolus. There were challenges in obtaining data for every HV and nerve. The sural nerve values for HV4 were negative (see inset image A in Figure 3) and the value for HV7 was near zero. The size of the sural nerve of HV4 was among the smallest, but HV7 was one of the larger (see Table 1), suggesting that size is not the only

15298027, 2024, 3, Downloaded from https://onlinelibrary.wiley.com/doi/10.1111/jns.12645 by Test, Wiley Online Library on [13/09/2024]. See the Terms and Conditions (https://onlinelibrary.wiley.com/terms-and-conditions) on Wiley Online Library for rules of use; OA articles are governed by the applicable Creative Commons License

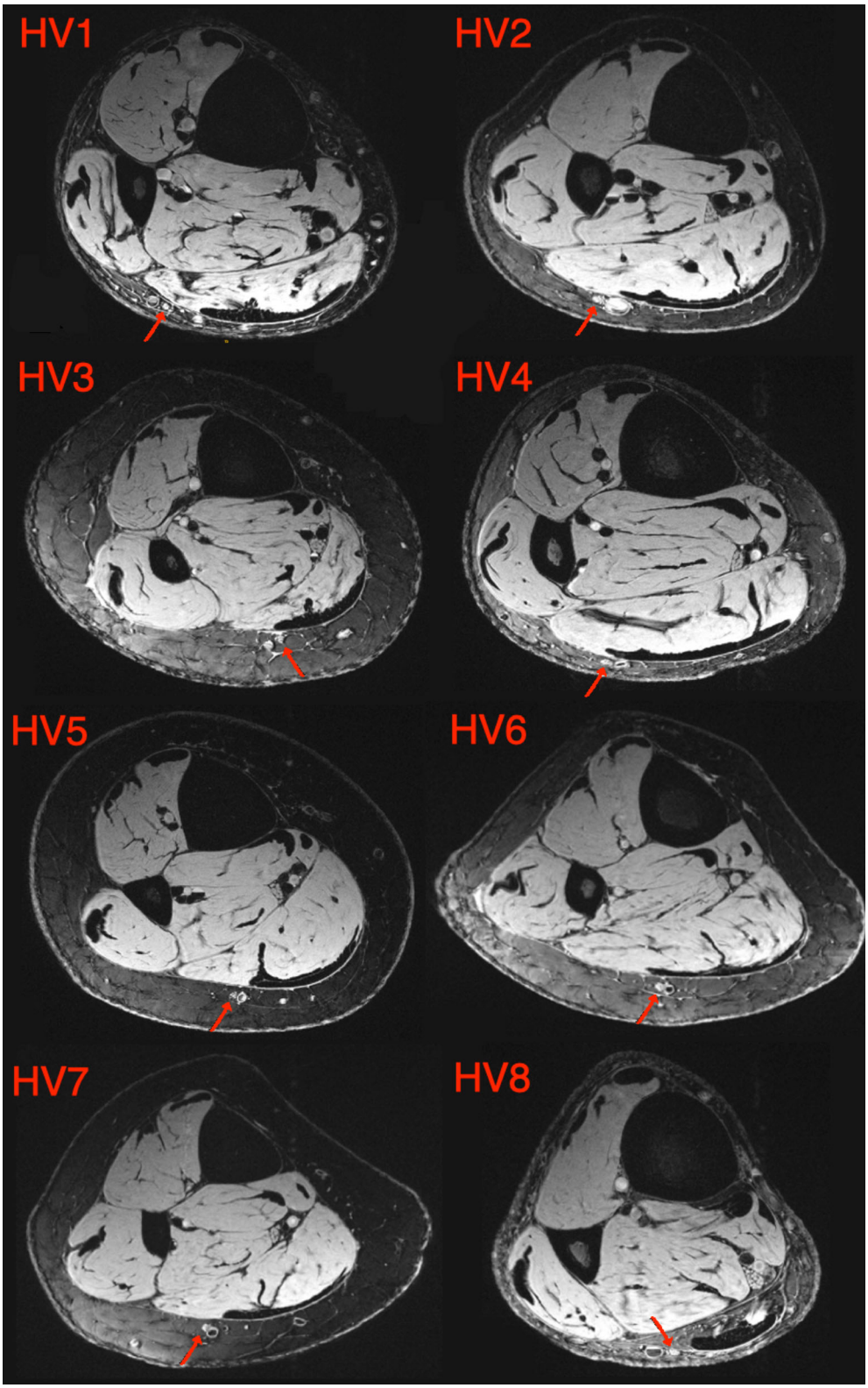



**FIGURE 1** Axial high-resolution double-echo in steady-state (DESS) images 7.2 cm above the lateral malleolus (the usual site for biopsy) from all eight participants. Images were chosen to demonstrate the location and relationship of the sural nerve (red arrows) and small saphenous vein. HV, healthy volunteer.

difficulty in obtaining quantitative measures at this level but also may still be a factor as the data for the much larger tibial nerve were consistently positive. The mean ± SD MTR values for the sural nerve were 0.11 ± 0.07, tibial 0.22 ± 0.03 and deep peroneal 0.20 ± 0.02. However, the deep peroneal nerve could only be seen on four of the HVs at the 7 cm landmark. Individual values are shown in Table S1.

## 4 | DISCUSSION

At 7T, and with clinically applicable sequences, we postulated that we would be able to image peripheral sensory nerves to almost their most distal extent and to sites where they might be amenable to biopsy for pathological diagnosis when this was required.

15298027, 2024, 3, Downloaded from https://onlinelibrary.wiley.com/doi/10.1111/jns.12645 by Test, Wiley Online Library on [13/09/2024]. See the Terms and Conditions (https://onlinelibrary.wiley.com/terms-and-conditions) on Wiley Online Library for rules of use; OA articles are governed by the applicable Creative Commons License

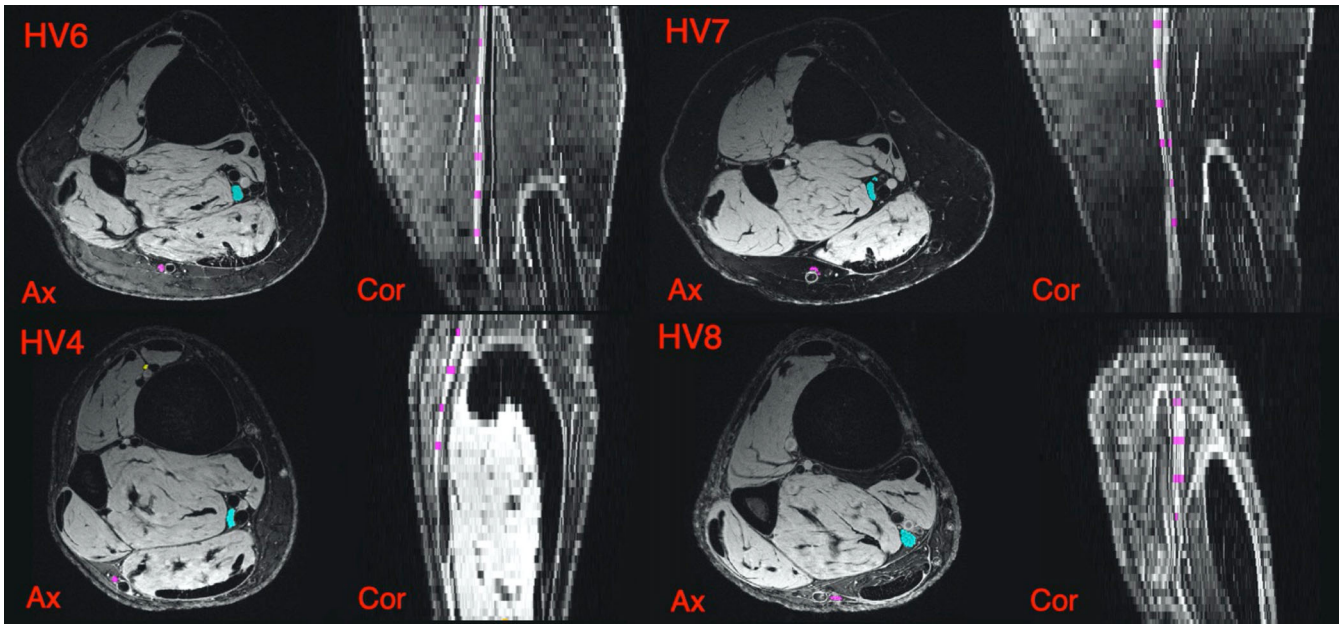



**FIGURE 2** Four example images in the axial (Ax; left) and coronal (Cor; right) planes. Tibial (blue), deep peroneal (yellow, only seen on healthy volunteer [HV] 4) and sural nerve (pink) are shown highlighted. The axial plane is placed at 7.2 cm above the malleolus. The coronal images show the sural nerve path traced in pink.

**TABLE 1** Summary of the systematic scoring concentrating on the area around the landmark 7.2 cm from the lateral malleolus.

| | | | Distances from malleolus in millimetres | | | |
|---|---|---|---|---|---|---|
| | | | 60 | 72 | 84 | 96 |
| HV1 | Tibial nerve | Est no. of fascicles | 13 | 15 | 16 | 14 |
| | | CSA ($mm^2$/voxel count) | 13.7/311 | 15.7/357 | 16/363 | 13.7/312 |
| | | Diameter (mm) | 4.4 | 4.1 | 4.3 | 4.3 |
| | | Relative to tibial vessels | Anterior | Anteromedial | Anteromedial | Medial |
| | | Relative to nearby muscle | Between FDL and FHL | Between FDL and FHL | Between FDL and FHL | Between FDL and FHL |
| | Sural nerve | CSA ($mm^2$/voxel count) | 3.6/82 | 3.6/81 | 3.4/77 | 3.3/76 |
| | | Diameter (mm) | 1.9 | 1.8 | 1.7 | 1.9 |
| | | Relative to SS vein | Posteromedial | Posteromedial | Posteromedial | Posteromedial |
| | | Relative to closest muscle | Overlying soleus | Overlying soleus | Overlying soleus | Overlying soleus |
| HV2 | Tibial nerve | Est no. of fascicles | 21 | 19 | 20 | 18 |
| | | CSA ($mm^2$/voxel count) | 19.9/452 | 18.5/420 | 18.3/415 | 17.1/388 |
| | | Diameter (mm) | 5.9 | 5.6 | 4.9 | 4.7 |
| | | Relative to tibial vessels | Medial | Medial | Medial | Posteromedial |
| | | Relative to nearby muscle | Between FDL and FHL | Between FDL and FHL | Between FDL and FHL | Between FDL and FHL |
| | Sural nerve | CSA ($mm^2$/voxel count) | 8.4/191 | 9/204 | 6.6/151 | 8.5/193 |
| | | Diameter (mm) | 3 | 3.1 | 2.9 | 2.9 |
| | | Relative to SS vein | Lateral | Lateral | Lateral | Lateral |
| | | Relative to closest muscle | Overlying soleus | Overlying soleus | Overlying soleus | Overlying soleus |
| HV3 | Tibial nerve | Est no. of fascicles | 19 | 19 | 20 | 16 |
| | | CSA ($mm^2$/voxel count) | 15.6/358 | 16.5/374 | 16.9/384 | 15.9/362 |
| | | Diameter (mm) | 3.9 | 4.1 | 3.9 | 3.8 |
| | | Relative to tibial vessels | Posterior | Posterior | Posterior | Posterior |

15298027, 2024, 3, Downloaded from https://onlinelibrary.wiley.com/doi/10.1111/jns.12645 by Test, Wiley Online Library on [13/09/2024]. See the Terms and Conditions (https://onlinelibrary.wiley.com/terms-and-conditions) on Wiley Online Library for rules of use; OA articles are governed by the applicable Creative Commons License

**TABLE 1** (Continued)

| | | | Distances from malleolus in millimetres | | | |
|---|---|---|---|---|---|---|
| | | | 60 | 72 | 84 | 96 |
| | | Relative to nearby muscle | Between FDL, FHL and soleus | Between FDL, FHL and soleus | Between FHL and soleus, posterior to FDL | Between FDL, FHL and soleus |
| | Sural nerve | CSA ($mm^2$/voxel count) | 4.3/98 | 4.1/93 | 4.4/99 | 4.4/101 |
| | | Diameter (mm) | 1.9 | 2.1 | 2.1 | 2.4 |
| | | Relative to SS vein | Medial | Medial | Anteromedial | Anteromedial |
| | | Relative to closest muscle | Overlying soleus | Overlying soleus | Overlying soleus | Overlying soleus |
| HV4 | Tibial nerve | Est no. of fascicles | 22 | 25 | 22 | 20 |
| | | CSA ($mm^2$/voxel count) | 15.9/361 | 16.1/366 | 17.2/392 | 16.5/375 |
| | | Diameter (mm) | 5.4 | 5.4 | 5.3 | 5.4 |
| | | Relative to tibial vessels | Posterolateral | Posterolateral | Posterolateral | Posterolateral |
| | | Relative to nearby muscle | Between FDL and FHL, posterior to Tib Post | Between FDL and FHL, posterior to Tib Post | Between FDL and FHL, posterior to Tib Post | Between FDL and FHL, posterior to Tib Post |
| | Sural nerve | CSA ($mm^2$/voxel count) | 3.4/78 | 3.4/78 | 2.8/64 | 3.3/76 |
| | | Diameter (mm) | 1.8 | 1.7 | 1.6 | 1.7 |
| | | Relative to SS vein | Anterolateral | Anterolateral | Anterolateral | Lateral |
| | | Relative to closest muscle | Overlying fascia between soleus and peroneus | Overlying soleus | Overlying soleus | Overlying soleus |
| HV5 | Tibial nerve | Est no. of fascicles | 16 | 15 | 16 | 17 |
| | | CSA ($mm^2$/voxel count) | 12.5/283 | 11.7/265 | 12.9/292 | 12/273 |
| | | Diameter (mm) | 4 | 4.1 | 4.2 | 4.6 |
| | | Relative to tibial vessels | Posteromedial | Posteromedial | Posteromedial | Posteromedial |
| | | Relative to nearby muscle | Between FLD and FHL, posterior to Tib Post | Between FHL and Tib Post | Between FHL and Tib Post | Between FHL and Tib Post |
| | Sural nerve | CSA ($mm^2$/voxel count) | 2.8/64 | 3.2/73 | 2.9/66 | 2.9/66 |
| | | Diameter (mm) | 1.7 | 1.9 | 1.7 | 1.7 |
| | | Relative to SS vein | Lateral | Lateral | Lateral | Lateral |
| | | Relative to closest muscle | Overlying soleus | Overlying soleus | Overlying soleus | Overlying soleus |
| HV6 | Tibial nerve | Est no. of fascicles | 24 | 24 | 20 | 21 |
| | | CSA ($mm^2$/voxel count) | 18/408 | 18.1/412 | 18/409 | 16.7/379 |
| | | Diameter (mm) | 4.1 | 4.3 | 4.5 | 4.5 |
| | | Relative to tibial vessels | Posterior | Posterior | PosteroLateral | PosteroLateral |
| | | Relative to nearby muscle | Between FDL and FHL | Between FDL and FHL | Between FDL and FHL | Between FDL and FHL |
| | Sural nerve | CSA ($mm^2$/voxel count) | 6.1/139 | 4.8/108 | 4.7/106 | 4.8/110 |
| | | Diameter (mm) | 2.3 | 2.1 | 2.1 | 2.1 |
| | | Relative to SS vein | Lateral | Lateral | Lateral | Lateral |
| | | Relative to closest muscle | Overlying soleus | Overlying soleus | Overlying soleus | Overlying soleus |
| HV7 | Tibial nerve | Est no. of fascicles | 25 | 24 | 25 | 25 |
| | | CSA ($mm^2$/voxel count) | 14.9/339 | 15.8/359 | 15.3/348 | 13.9/317 |
| | | Diameter (mm) | 5.1 | 5 | 4.6 | 5 |
| | | Relative to tibial vessels | Lateral | Lateral | Lateral | Lateral |
| | | Relative to nearby muscle | Between FDL and FHL, posterior to Tib post | Between FDL and FHL, posterior to Tib post | Between FHL and Tib post | Between FHL and Tib post |
| | | CSA ($mm^2$/voxel count) | 4.4/101 | 4.4/99 | 4.9/111 | 5.3/121 |

(Continues)

15298027, 2024, 3, Downloaded from https://onlinelibrary.wiley.com/doi/10.1111/jns.12645 by Test, Wiley Online Library on [13/09/2024]. See the Terms and Conditions (https://onlinelibrary.wiley.com/terms-and-conditions) on Wiley Online Library for rules of use; OA articles are governed by the applicable Creative Commons License

**TABLE 1** (Continued)

| | | | Distances from malleolus in millimetres | | | |
|---|---|---|---|---|---|---|
| | | | 60 | 72 | 84 | 96 |
| | Sural nerve | Diameter (mm) | 2.6 | 2.4 | 3.1 | 2.7 |
| | | Relative to SS vein | Anteromedial | Anteromedial | Anterior | Anterior |
| | | Relative to closest muscle | Overlying fascia between soleus and peroneus | Overlying soleus | Overlying soleus | Overlying soleus |
| HV8 | Tibial nerve | Est no. of fascicles | 28 | 27 | 25 | 27 |
| | | CSA ($mm^2$/voxel count) | 26.4/599 | 25.9/589 | 25.9/589 | 24.2/551 |
| | | Diameter (mm) | 5.1 | 5.5 | 5.5 | 5.4 |
| | | Relative to tibial vessels | Posterior | Posterior | Posterior | Posterolateral |
| | | Relative to nearby muscle | Between FDL and FHL | Between FDL and FHL | Between FDL and FHL | Between FDL and FHL |
| | Sural nerve | CSA ($mm^2$/voxel count) | 6.2/141 | 5.9/135 | 6.6/149 | 6.6/150 |
| | | Diameter (mm) | 2.7 | 3.4 | 3.4 | 3.3 |
| | | Relative to SS vein | Medial | Medial | Medial | Medial |
| | | Relative to closest muscle | Overlying soleus | Overlying soleus | Overlying soleus | Overlying soleus |

Abbreviations: CSA, cross-sectional area; EHL, extensor hallucis longus; FDL, flexor digitorum longus; FHL, flexor hallucis longus; HV, healthy volunteer; SS, small saphenous; Tib Post, tibialis posterior.

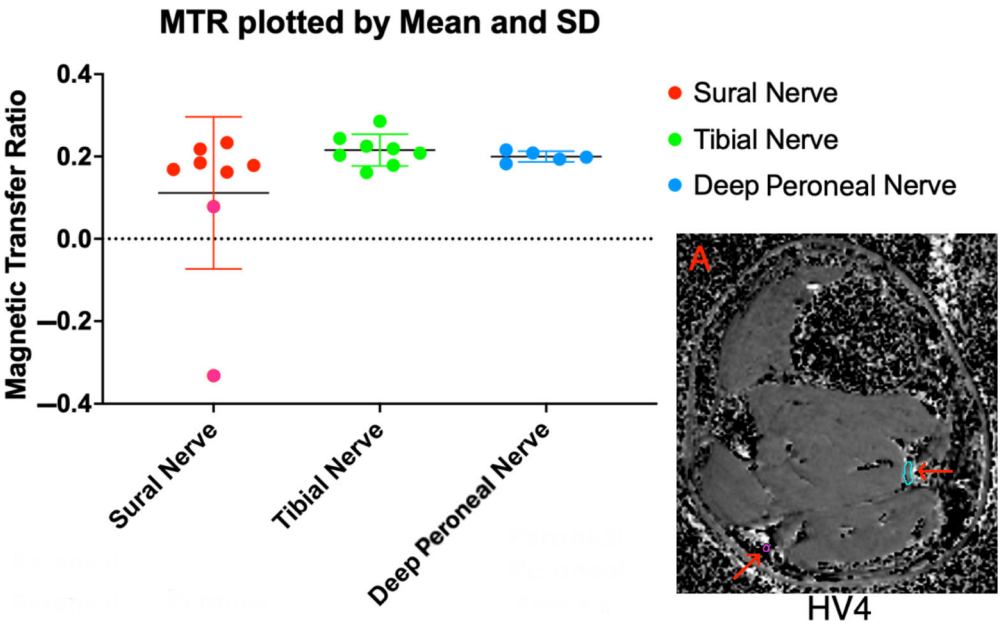



**FIGURE 3** Scatter plots of MTR values in the sural, tibial and deep peroneal nerve. The deep peroneal nerve was only seen in four of the volunteers at the level of 7 cm above the malleolus. The inset image A shows example regions of interests (ROIs) drawn in healthy volunteer (HV) 7 in the tibial nerve (blue) and sural nerve (pink). In this image however, no signal is seen in the pink sural nerve ROI.

We have proven the feasibility of imaging the distal lower leg at 7T for visualising the sural nerve. We have mapped the anatomical variation of in vivo non-cadaveric peripheral nerves and have shown that the sural nerve is variable in anatomical site as well as its relationship to the adjacent vein in life. Imaging was optimised for the visualisation of the sural nerve and so analysis of the superficial peroneal nerve was not possible. Future work would include imaging both the sural and superficial peroneal nerves in both legs for full MR validation. However, we have identified that the tibial nerve is particularly well visualised, and although it was not the target of our project, more normative- and disease-related information would be likely to be assessable from this nerve in the future.

We have also measured the vital imaging characteristics in a series of applicable MRI sequences with a view to obtaining data on normal values and normal variation before applying the technique to pathological nerves planned for diagnostic biopsy. The variation in these characteristics within the small sural nerve is potentially too great to utilise MRI at 7T with these sequences for histopathological quantification and correlation. However, in the future, we will correlate in vivo imaging features of pathological nerves to the ex vivo histopathology findings to correlate the signal characteristics and features that might improve diagnosis and potentially reduce morbid procedures for patients. This would need to be performed in a larger

15298027, 2024, 3, Downloaded from https://onlinelibrary.wiley.com/doi/10.1111/jns.12645 by Test, Wiley Online Library on [13/09/2024]. See the Terms and Conditions (https://onlinelibrary.wiley.com/terms-and-conditions) on Wiley Online Library for rules of use; OA articles are governed by the applicable Creative Commons License

control/patient cohort to establish normal and pathological ranges as the opportunity to biopsy relevant pathologies presents infrequently, and the diagnosis would only be known after the biopsy.

The results of the MTR analysis in the sural nerve were not found to be consistent in all volunteers, and this may not make a suitable measurement in individual patients or in clinical trials where measurements must be reliable and reproducible often without expert assistance. The deep peroneal nerve is the same order of size as the sural nerve but, where seen, had consistent MTR values. However, it is positioned rather close to muscle, whereas the sural nerve is embedded in fat possibly affecting the acquisition, although HV4 did have one of the smaller quantities of superficial fat of the cohort. Fat suppressed MTR imaging may provide more consistency when imaging the sural nerve, such as correction with a water image derived from the three-point Dixon method.[12,13] This will likely require advanced sequence development on a 7T research scanner. The larger tibial nerve values were consistent however, but would need to be compared between pathological and healthy nerves to ensure that the healthy values are grouped tightly enough to show any differences in health and disease and level of significance when tested.

In the future, we wish to measure other quantitative MR indices such as T2 and diffusion in these peripheral nerves. Given that the pathology identified (via biopsy) in the sural and superficial peroneal nerve is likely to be similar to the pathology in the distal tibial nerve in most pathological sensorimotor neuropathies, it may be that indirect correlations can be drawn between the MRI imaging characteristics of the tibial nerve and the pathological findings on biopsy. Future work could include comparing MR indices in the pathological sural nerve to those in the tibial nerve or sciatic nerve to establish criteria for diagnosis in those larger nerves that can be detected at lower field strengths and so remove the need for biopsy. This could be complemented by large coverage or whole-body imaging at 3T for example, to view systemic disease for diagnosis instead of relying on detecting disease in those small superficial nerves suitable for biopsy. Substantial studies with histological validation of MR are required first and normative ranges of MR indices in these small nerves, challenging to image at 3T, must be established as a foundation. To this end, we are developing quantitative MR sequences separate to DESS such as diffusion tensor imaging at this time.

## ACKNOWLEDGEMENTS

This study was generously funded by Muscular Dystrophy UK and supported by researchers at the National Institute for Health and Care Research University College London Hospitals Biomedical Research Centre. Michael P. Lunn is supported by the NIHR Biomedical Research Centre at University College London Hospitals NHS Foundation Trust and University College London. Amy R. McDowell and Laura Zambreanu both contributed equally to the article.

## DATA AVAILABILITY STATEMENT

The data that support the findings of this study are available on request from the corresponding author. The data are not publicly available due to privacy or ethical restrictions.

## ORCID

*Amy R. McDowell* https://orcid.org/0000-0002-4886-6191
*Carolynne M. Doherty* https://orcid.org/0000-0003-0129-3573
*Michael P. Lunn* https://orcid.org/0000-0003-3174-6027

## REFERENCES

1. Jackson LJ, Serhal M, Omar IM, Garg A, Michalek J, Serhal A. Sural nerve: imaging anatomy and pathology. *Br J Radiol*. 2023;96:20220336.
2. Zaidman CM, Seelig MJ, Baker JC, Mackinnon SE, Pestronk A. Detection of peripheral nerve pathology: comparison of ultrasound and MRI. *Neurology*. 2013;80:1634-1640.
3. Koneru S, Nguyen VT, Hacquebord JH, Adler RS. Brachial plexus nerve injuries and disorders: MR imaging-ultrasound correlation. *Magn Reson Imaging Clin N Am*. 2023;31(2):255-267.
4. Abreu E, Aubert S, Wavreille G, Gheno R, Canella C, Cotten A. Peripheral tumor and tumor-like neurogenic lesions. *Eur J Radiol*. 2013;82(1):38-50.
5. Elston DM. Confirmation bias in medical decision-making. *J Am Acad Dermatol*. 2020;82:572.
6. Kollmer J, Hund E, Hornung B, Hegenbart U, Schönland SO, Kimmich C, Kristen AV, Purrucker J, Röcken C, Heiland S, Bendszus M, Pham M. In vivo detection of nerve injury in familial amyloid polyneuropathy by magnetic resonance neurography. *Brain*. 2015;138(Pt 3):549-562.
7. Sveinsson B, Rowe OE, Stockmann JP, et al. Feasibility of simultaneous high-resolution anatomical and quantitative magnetic resonance imaging of sciatic nerves in patients with Charcot-Marie-tooth type 1A (CMT1A) at 7T. *Muscle Nerve*. 2022;66:206-211.
8. Mahakkanukrauh P, Chomsung R. Anatomical variations of the sural nerve. *Clin Anat*. 2002;15:263-266.
9. Yoon D, Biswal S, Rutt B, Lutz A, Hargreaves B. Feasibility of 7T MRI for imaging fascicular structures of peripheral nerves. *Muscle Nerve*. 2018;57:494-498.
10. Schreiber S, Schreiber F, Peter A, et al. 7T MR neurography-ultrasound fusion for peripheral nerve imaging. *Muscle Nerve*. 2020;61:521-526.
11. Gold GE, Hargreaves BA, Reeder SB, et al. Balanced SSFP imaging of the musculoskeletal system. *J Magn Reson Imaging*. 2007;25:270-278.
12. Li W, Wang X, Miller FH, Larson AC. Chemical shift magnetization transfer magnetic resonance imaging. *Magn Reson Med*. 2017;78:656-663.
13. Smith AK, Dortch RD, Dethrage LM, et al. Incorporating dixon multi-echo fat water separation for novel quantitative magnetization transfer of the human optic nerve in vivo. *Magn Reson Med*. 2017;77:707-716.

## SUPPORTING INFORMATION

Additional supporting information can be found online in the Supporting Information section at the end of this article.

**How to cite this article:** McDowell AR, Zambreanu L, Salhab HA, et al. Initial findings using high-resolution magnetic resonance imaging for visualisation of the sural nerve and surrounding anatomy in healthy volunteers at 7 Tesla. *J Peripher Nerv Syst*. 2024;29(3):368-375. doi:10.1111/jns.12645

15298027, 2024, 3, Downloaded from https://onlinelibrary.wiley.com/doi/10.1111/jns.12645 by Test, Wiley Online Library on [13/09/2024]. See the Terms and Conditions (https://onlinelibrary.wiley.com/terms-and-conditions) on Wiley Online Library for rules of use; OA articles are governed by the applicable Creative Commons License